ELSEVIER

Chemical Engineering Journal 130 (2007) 1–10

Chemical Engineering Journal

www.elsevier.com/locate/cej

Heat transfer of gas–solid two-phase mixtures flowing through a packed bed under constant wall heat flux conditions

Thang Ngoc Cong [a], Yurong He [a], Haisheng Chen [a], Yulong Ding [a,*], Dongsheng Wen [b]

[a] *Institute of Particle Science and Engineering, University of Leeds, Leeds LS2 9JT, UK*
[b] *Department of Engineering, Queen Mary University of London, Mile End, London E1 4NS, UK*

Received 13 July 2006; received in revised form 13 November 2006; accepted 15 November 2006

Abstract

An experimental study has been carried out on both the transient and steady state heat transfer of a gas–solid two-phase mixture flowing through a cylindrical packed bed reactor under the constant wall heat flux conditions. A logarithmic mean temperature difference (LMTD) method is used to process the steady state data to obtain the overall heat transfer coefficient. The effects of solids loading, particle size and flow Reynolds number are investigated. The results show that the introduction of suspended particles greatly enhances the heat transfer and the enhancement increases approximately linearly with solids loading and the effect of particle size is relatively weak under the conditions of this work. A correlation is proposed based on the experimental data, which relates well the Nusselt number to the Reynolds number, the Archimedes number and the suspended solids loading. Given other conditions, the Nusselt number at the constant wall heat flux conditions is much higher than that under the constant wall temperature conditions. It is shown that the Reynolds number and particle loading have a greater influence on the Nusselt number under the constant heat flux conditions than that under the constant wall temperature conditions investigated by the authors in a previous study.

Keywords: Heat transfer; Gas–solid mixtures; Two-phase flow; Packed bed; Constant wall heat flux

1. Introduction

Gas–solid two-phase mixtures flowing through packed beds are important to a number of industrial processes including waste heat recovery and filtration of dusty flue gases, adsorption of gas components from dust laden gases, pulverized coal gasification and combustion and some newly proposed chemical reactors using solids circulation [1]. Heat transfer can play a crucial role in determining the performance of these processes. Although numerous reports can be found from the literature on the heat transfer behaviour of single gas phase flowing through packed beds [2–9] and gas–solid two-phase mixtures flowing through empty pipes [10–14], very few studies have been carried out on the heat transfer between gas–solid two-phase mixtures and packed beds. Royston [15] investigated heat transfer between a vertical column packed with 6.35 mm stainless steel particles and a downward flowing gas–solid suspension. The packed column was made of glass and had an internal diameter of 76 mm and a height of 178 mm. Zircon, ilmenite, glass ballotini and a catalyst ranging from 68 to 245 μm were used as suspended particles. The experiments were performed with different loadings of fine particles in the gas at a Reynolds number ranging from 840 to 1400. The results showed a significant enhancement of heat transfer in comparison with single gas phase cases and the enhancement ratio related well to the ratio of $G_s c_s/G_g c_g$ in a linear fashion:

$$\frac{h_m}{h_g} = 0.26\frac{G_s c_s}{G_g c_g} + 1, \qquad \frac{G_s}{G_g} = 0\text{–}6 \tag{1}$$

with h_m and h_g are the heat transfer coefficients of gas–solid two-phase and single gas phase flows, G_s and G_g the solids and gas flow mass fluxes, and c_s and c_g are the solids and gas phase heat capacities, respectively. The enhancement ratio, however, was found to be insensitive to the gas Reynolds number and other properties of suspended particles, such as particle size, density and thermal conductivity.

* Corresponding author. Tel.: +44 113 343 2747; fax: +44 113 343 2405.
E-mail address: y.ding@leeds.ac.uk (Y. Ding).

1385-8947/$ – see front matter © 2006 Elsevier B.V. All rights reserved.
doi:10.1016/j.cej.2006.11.006

Nomenclature

A_{ht}	heat transfer area (m^2)
Ar_m	Archimedes number defined as $Ar_m = d_p^3 g\rho_g(\rho_p - \rho_g)(1-\varepsilon)^2/\mu_g^2$
c_g	gas specific heat (J/(kg K))
c_s	solids phase specific heat (J/(kg K))
d_p	packed particle diameter (m)
g	gravitational acceleration (m/s^2)
G_g	gas flow flux ($kg/(m^2\ s)$)
G_s	suspended solids flux ($kg/(m^2\ s)$)
h_g	heat transfer coefficient of pure gas flow ($W/(m^2\ K)$)
h_m	heat transfer coefficient of gas–solid two-phase flow ($W/(m^2\ K)$)
k_f	fluid thermal conductivity (W/(m K))
m_g	gas flowrate (kg/s)
m_i	solids flowrate (kg/s)
Nu_m	Nusselt number defined as $Nu_m = h_m d_p/k_f$
Q	heat flux (W)
Re_p	Reynolds number defined as $Re_p = \rho_g v_g d_p/\mu_g$
T_{ap}	average temperature of the packed bed and the column wall (°C)
T_{ax}	temperature at the column centre (°C)
T_g	gas phase temperature (°C)
T_s	solids phase temperature (°C)
T_w	temperature of the outer surface of the column wall (°C)
T_0	temperature at the bed inlet (°C)
$(\Delta T)_{lm}$	logarithmic mean temperature difference
v_g	superficial gas velocity (m/s)
z	axial distance (m)

Greek letters

ε	voidage
Φ_s	particle shape factor
μ_g	gas phase viscosity (kg/ms)
ρ_g	gas phase density (kg/m^3)
ρ_p	suspended solids phase density (kg/m^3)

Subscripts

in	inlet
out	outlet

Balakrishnan and Pei [16–18] performed experiments with a 50.8 mm diameter Pyrex glass column packed with particles to a height of 48 mm. Different shapes of iron oxide, nickel oxide and two types of vanadium pentoxides with equivalent diameters between 5.5 and 12.7 mm were used as packed particles. Spherical glass beads with 100, 150 and 250 μm diameters were used as suspended particles and a microwave heating method was used to supply heat to the bed. The experiments were carried out at a Reynolds number ranging from 400 to 1400 and a large increase in the heat transfer coefficient was observed in comparison with the single gas phase flow cases and the enhancement was shown to relate linearly to the ratio of G_s/G_g:

$$\frac{h_m}{h_g} = 0.25\frac{G_s}{G_g} + 1, \qquad \frac{G_s}{G_g} = 0.9\text{–}5.4 \tag{2}$$

The data of the convective heat transfer coefficient were also processed to give the Nusselt number (Nu_m) which was then correlated to particle Reynolds number (Re_p), Archimedes number (Ar_m), solids loading and the shape factor of the packing materials:

$$Nu_m = 0.016 Ar_m^{0.25}\ Re_p^{0.5}\left(1 + \frac{G_s}{G_g}\right)^{0.68}\Phi_s^{3.76} \tag{3}$$

where

$$Nu_m = \frac{h_m d_p}{kf}, \qquad Re_p = \frac{\rho_g v_g d_p}{\mu_g},$$

$$Ar_m = \frac{d_p^3 g\rho_g(\rho_p - \rho_g)(1-\varepsilon)^2}{\mu_g^2},$$

ρ_g and ρ_p, respectively, the gas and solids densities, g the gravitational acceleration, μ_g the gas phase viscosity, ε the voidage, d_p the packed particle diameter, Φ_s the particle shape factor, k_f the fluid conductivity and v_g the superficial gas velocity.

Wen et al. [19] investigated experimentally the heat transfer of a gas–solid two-phase mixture flowing vertically upwards through a long packed column under the constant wall temperature conditions. Glass beads with 112.5 μm diameter were used as suspended particles. The experiments were done with a solid-to-gas mass flux ratio (G_s/G_g) ranging from 0.05 to 2 at a Reynolds number between 149 and 335. Processing of the data with the logarithmic mean temperature difference (LMTD) method gave similar relationships to Eqs. (1)–(3), but the prefactors are significantly different:

$$\frac{h_m}{h_g} = 0.69\frac{G_s}{G_g} + 1 \tag{4a}$$

$$\frac{h_m}{h_g} = 0.85\frac{G_s c_s}{G_g c_g} + 1 \tag{4b}$$

$$Nu_m = 0.0053 Ar_m^{0.25}\ Re_p^{0.5}\left(1 + \frac{G_s}{G_g}\right)^{0.68} \tag{5}$$

The data obtained by Royston [15] include contributions from both the convection and conduction components due to non-uniform temperature distribution in the packed bed. Balakrishnan and Pei [16–18] claimed to have achieved a uniform temperature distribution due to the use of microwaving heating so their data consisted of only the convection contribution. However, the bed height used by Balakrishnan and Pei [16–18] was very short due to the limitation of the microwave facility. It is also noted that the data published by Royston [15] and Balakrishnan and Pei [16–18] are for particle Reynolds numbers over 400; while Wen et al. [19] investigated the heat transfer behaviour at a Reynolds number lower than ~400 with a long column and at the constant wall temperature conditions. However, some industrial processes are operated under constant heat flux conditions and/or at very low particle Reynolds numbers,

for which little work has been done. This forms the main motivation of the present work. An additional motivation of the work arises from an on-going study on low temperature hydrogen production using adsorption enhanced chemical reaction processes and solids circulating technology for which heat supply to the packed bed reactor and heat transfer within the bed are identified as two technical challenges [1,20,21].

2. Experiments

The experimental system used in this work is shown schematically in Fig. 1. It consisted of a packed column, a compressed air supply unit, a suspended particle collection tank, a suspended particle dispensing tank, a particle injection unit for introducing suspended particles into the packed bed, two cyclones in series for particle separation, and various flow and temperature measurement and control units. The solids flow was controlled by a Venturi type of device; see Wang et al. [20] and Ding et al. [1] for details. The gas flow was metered and controlled by mass flow controllers. Two RS pressure transducers were used to measure the pressure at the inlet and outlet of the packed bed. The pressure drop across the packed bed was also measured with a DM2L micro-manometer interfaced to a PC through an RS232 port.

The packed column used was the same as that used by Wen et al. [19]. It was made of stainless steel and had an internal diameter of 41 mm, an external diameter of 48 mm and a length of 1100 mm; see Fig. 2 for a schematic diagram. It was heated by a three-zone ceramic heater with each zone controlled independently (Watlow, UK). The three ceramic heaters were exactly

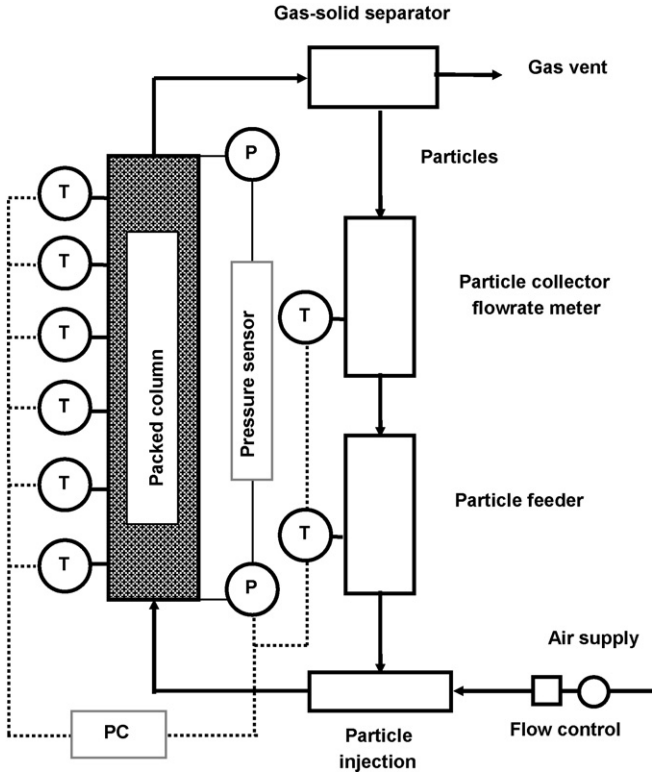

Fig. 1. Experimental system.

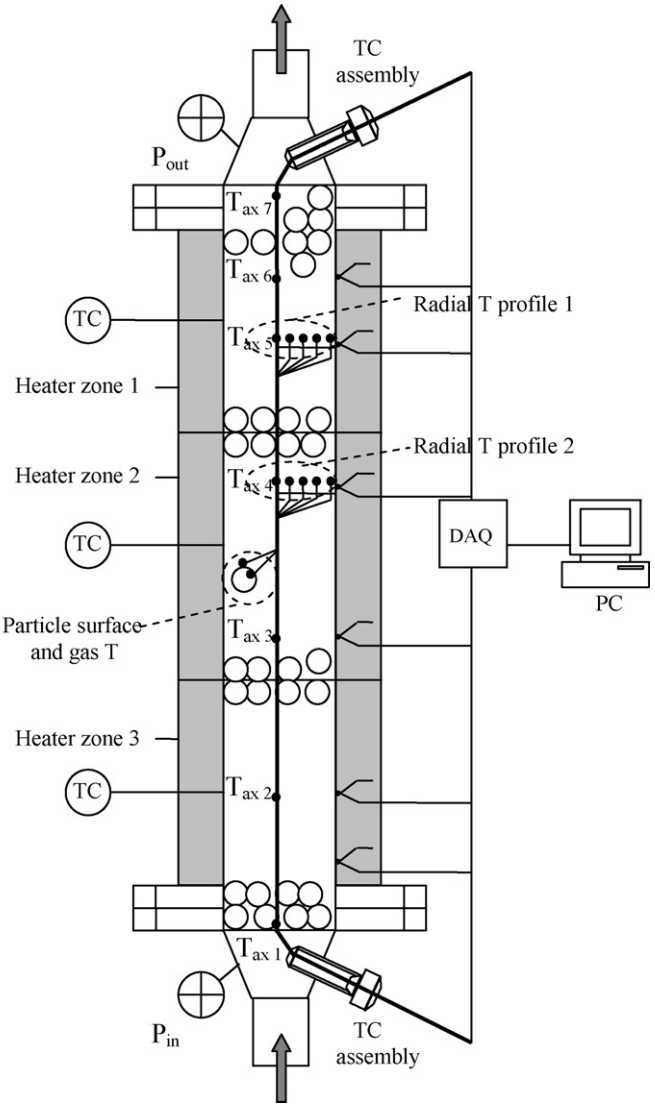

Fig. 2. Thermocouple arrangements of heat transfer experiments.

the same. The power supplied to the three heaters was exactly the same and was automatically controlled. The heaters were insulated with ~50 mm thickness porous insulation materials and the inlet and outlets of reactor were insulated with similar porous insulation materials. As the insulation materials and their thickness were exactly the same, they were expected to produce the same extent of insulation. As the thickness of the external insulation was ~50 mm, the heat loss to the surrounding was negligible. The conduction of the stainless steel wall in the axial direction was estimated to be over three orders of magnitude smaller than that in the radial direction, which was therefore negligible.

Glass balls with 5 ± 0.3 mm diameter were randomly packed into the column. Two thermocouple assemblies (TC Direct, UK), each consisting of 12 Type J sheathed thermocouples were used to measure the temperature field in the interior of the packed bed. These thermocouples had a diameter of 0.25 mm thus contributed very little to heat conduction. A 1 mm stainless steel rod with two radial supporting arms (1 mm) was inserted in the

central part of the column to position the thermocouples. The thermocouples were carefully wired along the rod with thermocouple tips protruding into the bed side to ensure that they were bathed in the surrounding flow. Particular attention was also paid to connecting the thermocouple wires to the data acquisition system through the supporting rod to minimise disturbance to the flow and temperature fields. Axial temperature profile was measured in the column centre by seven thermocouples located at axial positions of 0, 188, 379, 579, 764, 964 and 1100 mm from the inlet, which corresponded to 0, 17.1, 34.4, 52.6, 87.6 and 100% relative to the total length of the column. Radial temperature profiles in two axial positions of 579 and 764 mm from the inlet were obtained by five thermocouples in each of the axial position, where the thermocouples were supported by the two tiny arms and located at radial positions of 0, 5, 10, 15 and 20 mm (corresponding to 0, 24.4, 48.8, 73.2 and 97.6% of the column radius). The external surface temperature of the packed bed was measured by seven thermocouples located in different axial and tangential positions to monitor the wall temperature uniformity. A thermocouple was also mounted onto the surface of a packed particle located approximately half way between the centre and the column wall, where another one was positioned nearby to measure the fluid temperature passing across the particle so that the temperature difference between the fluid and packed particles could be investigated. All temperature signals were collected by a data acquisition system (NI PCI-6052E) inside a PC. A SCXI-1102 32-channel thermocouple amplifier was used to achieve high accuracy of temperature measurements. A Labview software was used for system configuration and data logging.

Experiments were performed in both the transient and steady states under a constant heat flux of 12.71 kW/m^2. Spherical glass beads with 55 and 112.5 μm diameters were used as suspended particles. The particle sizes were obtained by the laser diffraction method. Suspended solids mass flux (G_s) was adjusted to range from 0.2 to 3.0 kg/(m^2 s) and the Reynolds number (Re_p) ranged from 149 to 373 where the viscosity was calculated at the average inlet and outlet temperatures. It typically took about 2 h (depending on the gas flowrate and solid loading) from the cold for the whole system to reach the steady state (defined as the period when the temperature profiles in the packed bed did not change with time). All thermocouples were calibrated before use and were found to have an accuracy of 0.2 K. Heat conduction through the stainless steel supporting rod and arms was very small due to the small diameter. As the temperature used in this work is typically below 120 °C, the radiation contributes to less than ∼1% of the overall heat transfer. The uncertainties of the gas flowrate and pressure drop measurements under the conditions of this work were estimated at 2 and 4%, respectively. The suspended particle concentration uncertainty was estimated to be better than 10%.

In a typical experiment from cold, heaters were switched on for sometime before the gas was introduced to warm up the bed. Once the bed reached its steady state under a specified gas flow rate, the suspended particles were introduced and the experiment continued until a new steady state was reached. For experiments with a hot start, i.e. the packed bed was hot due to previous experiments, a much short start-up period was needed before gas was introduced.

3. Results and discussion

3.1. Temperature profiles

3.1.1. Transient temperature profiles in the axial direction

Fig. 3(a) shows the temperature responses at different axial positions of the column centre to the introduction of the gas and the suspended particles (55 μm) for a cold start. The results for the 112.5 μm particles are similar. The gas flowrate was $G_g = 1.52$ kg/(m^2 s) and the solid-to-gas ratio was controlled at $G_s/G_g = 0.95$. The corresponding Reynolds number of the experiment was 373. The temperature data were recorded at a rate of 1 Hz, but are presented at an interval of 20 s for clarity. It can be seen that the temperatures at all axial positions are the same and equal to ∼16 °C before the heaters are switched on. Four stages can be identified from the figure, pre-heating stage, gas flow stage, gas–solid flow stage and post-gas–solid flow stage.

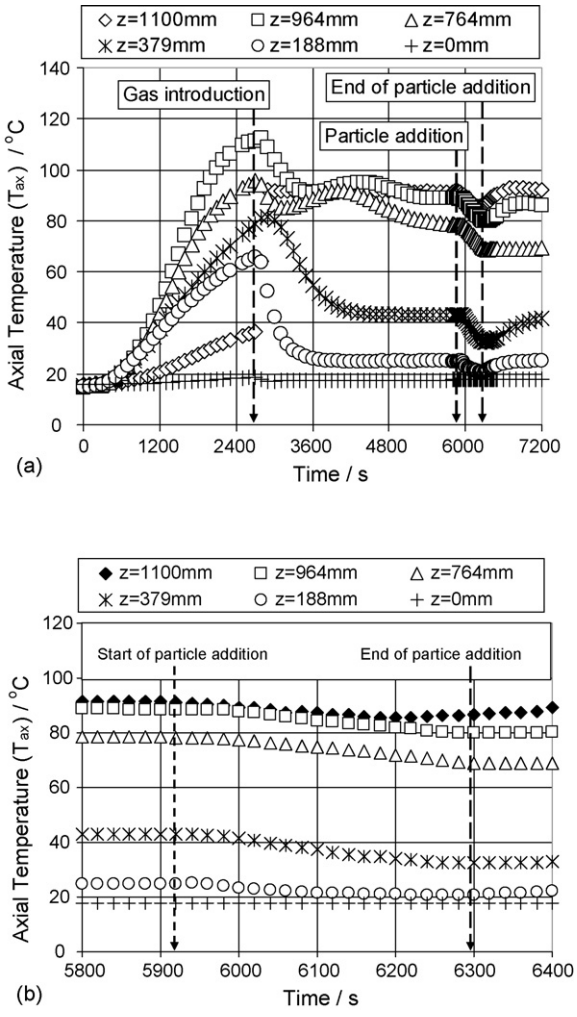

Fig. 3. Axial transient temperature profiles for $G_s/G_g = 0.95$, $Re_p = 373$, $G_g = 1.52$ kg/(m^2 s) and 55 μm glass beads: (a) temperature response over the four stages and (b) temperature response in the gas–solid flow stage.

In the pre-heating stage (time = 0–2500 s; Fig. 3(a)), the column centre temperature starts to increase rapidly in ~15 min after the heaters are switched on. Such a time delay indicates that the effective radial thermal diffusivity of the packed bed is $\sim 4.5 \times 10^{-7}$ m^2/s ((column radius)^2/delaying time); this is approximately of the same order of magnitude as that of the packed glass particles, suggesting that the conduction be the dominant mechanism during the pre-heating stage. The rate and extent of temperature increase are found to be dependent on the axial position; they increase with increasing axial position between $z = 0$ (inlet) and 964 mm (just below the exit). The temperature at the exit ($z = 1100$ mm), however, shows a low rate and extent of temperature increase possibly because the thermocouple at the position is located just outside the heated region and as a consequence the heat has to be supplied mainly through the natural convection of the gas.

When the gas flow is introduced (the gas flow stage) at time ~2500 s (Fig. 3(a)), the temperature at all axial positions except for $z = 1100$ mm decreases rapidly and a steady state is established at time ~4500 s. The temperature in the steady state increases with the axial position at $z = 0$–764 mm beyond which only small temperature change is seen, indicating that the packed bed approaches the thermally fully developed regime at $z \gtrsim 764$ mm. At $z = 1100$ mm, however, a steep temperature increase is observed when the gas flow is introduced, mainly due to the heat accumulated in the whole bed during the pre-heating stage being displaced through the exit of the bed. The steep temperature jump at $z = 1100$ mm in Fig. 3 is because not all the data points are shown to ensure the figure clarity. It is also noted that the time for reaching the steady state depends on the axial position; slower in the exit region (downstream) and faster in the lower part of the bed (upstream).

A rapid drop of the bed temperature is seen upon introduction of suspended particles at time = 5900 s (the gas–solid flow stage, Fig. 3(a)). Zooming in the temperature response in the gas–solid flow stage (Fig. 3(b)), one can see the bed reaches a new steady state upon introduction of particles much more quickly (within ~300 s) than that due to introduction of gas flow (within ~2000 s). The quicker approach to the steady state in the presence of suspended particles indicates a higher heat transfer coefficient between the flow and the packed bed. Note that temperature profiles shown in Fig. 3 are still seen to change with time when particle addition is ended. However, the change is very small and slow so the bed is in an approximately steady state.

When addition of suspended particles is stopped at time = 6300 s (Fig. 3(a)) and the gas flow is maintained, the temperature is seen to increase quickly to the level close to the value before suspended particles are introduced. The slight difference may be due to the existence of small amount of particles still in the bed. This part of particles is also called static hold-up [1,21] and requires a long purging time.

If the axial temperature distribution data as shown in Fig. 3 is made dimensionless according to $(T_{ax} - T_0)/(T_w - T_0)$, Fig. 4 is obtained for the period between the addition and the end of suspended particles at two solid-to-gas mass flux ratios of

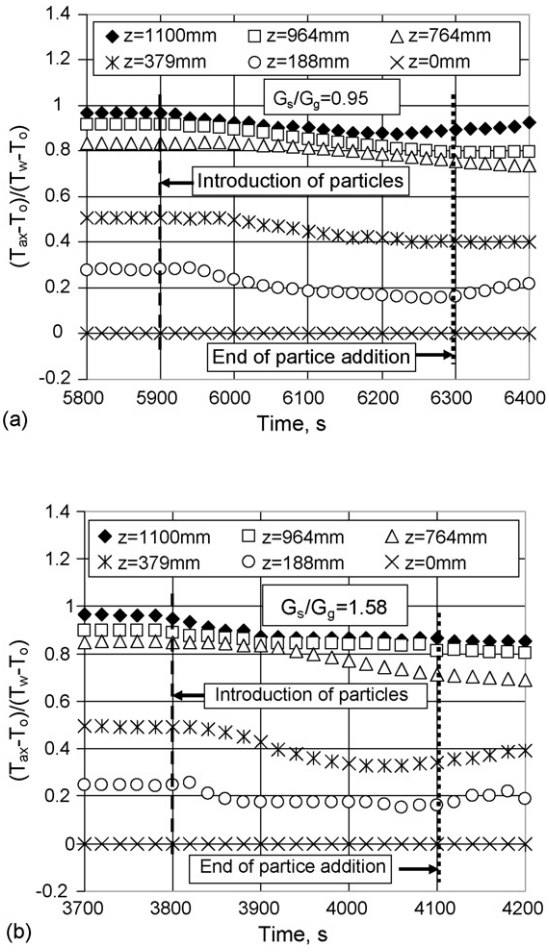

Fig. 4. Dimensionless transient temperature profiles at two solid-to-gas mass flux ratios: $Re_p = 373$, $G_g = 1.52$ kg/(m^2 s) and 55 μm glass beads: (a) $G_s/G_g = 0.95$ and (b) $G_s/G_g = 1.58$.

0.95 and 1.58, where T_{ax} is the temperature at the column centre, T_w the local wall temperature (outer surface of the column wall) and T_0 is the bed inlet temperature. An inspection of Fig. 4(a and b) shows that the addition of suspended particles at the higher solids flowrate gives a greater temperature drop and hence a lower temperature at the new steady state, which is mainly due to more heat being carried away by the suspended particles as well as more intensified convective heat transfer.

3.1.2. *Effect of radial position on the transient temperature profiles*

Fig. 5 compares the temperature profiles at two radial positions for $z = 579$ and 764 mm in the gas–solid flow stage (55 μm particles, two solids loadings). The results for 112.5 μm particles are similar. The addition of suspended particles leads to a decrease in the bed temperature, consistent with the observed axial temperature profiles (Section 3.1.1). A new steady state is established shortly after the introduction of solids. Given other conditions, a higher solid loading gives a shorter transition duration. The radial temperature distribution at $z = 579$ mm is less uniform than that at $z = 764$ mm, and the non-uniformity

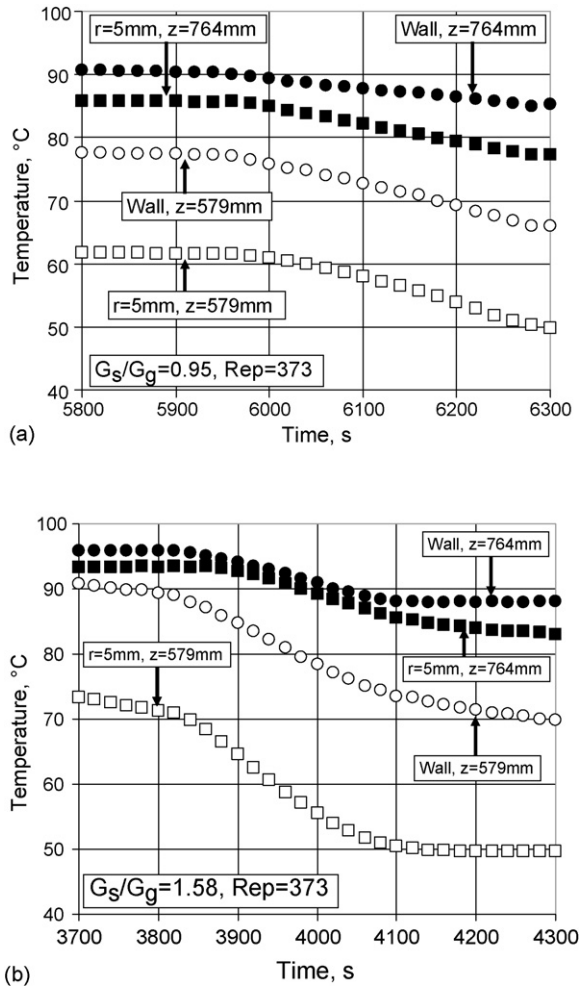

Fig. 5. Radial transient temperature profiles for $Re_p = 373$, $G_g = 1.52\ \mathrm{kg/(m^2\ s)}$ and 55 μm glass beads: (a) $G_s/G_g = 0.95$ and (b) $G_s/G_g = 1.58$.

increases with increasing solid loading, e.g. at $z = 579$ mm, the maximum temperature difference between $r = 5$ mm and the wall for $G_s/G_g = 1.58$ is ~20 °C, whereas that for $G_s/G_g = 0.95$ is only ~15 °C.

3.1.3. Transient temperature responses of the packed particle surface and surrounding fluid

Fig. 6 shows the temperature profiles measured by the thermocouple attached to the packed particle surface and the nearby thermocouple exposed in the fluid phase for $Re_p = 373$, $G_g = 1.52\ \mathrm{kg/(m^2\ s)}$ at two suspended particle loadings. The temperature profiles under other conditions are similar. The time shown in Fig. 6 has been re-scaled so that the data under different conditions can be presented in one graph. It can be seen that the introduction of suspended particles leads to a decrease in both the packed particle surface and fluid phase temperatures. However, the difference between the two temperatures is small at the location investigated. The maximum temperature difference between the packed particle surface and fluid phase is found to be ~0.5 K at $Re_p = 373$ and the difference increases slightly with increasing Reynolds number (data not shown).

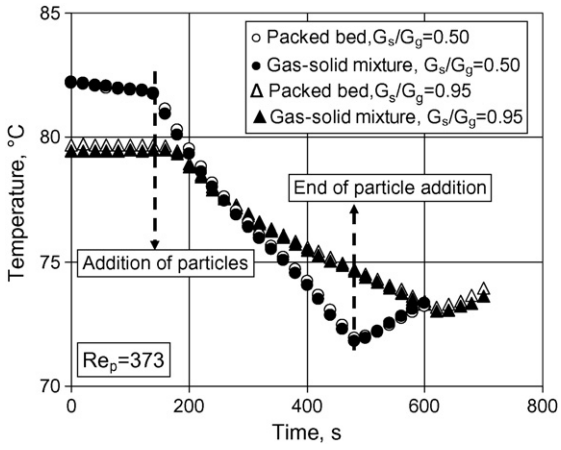

Fig. 6. Transient packed particle surface and fluid temperatures for $Re_p = 373$, $G_g = 1.52\ \mathrm{kg/(m^2\ s)}$ and 55 μm glass beads.

3.1.4. Steady state temperature profile

The steady state temperature expressed in the dimensionless form is plotted in Fig. 7 as a function of the axial position for various particle loadings of 55 μm particles at $Re_p = 373$ and $G_g = 1.52\ \mathrm{kg/(m^2\ s)}$. Similar results are observed under other conditions. The dimensionless temperature increases almost linearly with increasing axial distance for $z \lesssim 600$ mm beyond which the temperature levels off. This is different from the constant wall temperature results, which show an S-shaped curve with the dimensionless temperature increasing slowly initially for $z \lesssim 200$ mm, then rapidly for $z \cong 200$–650 mm and finally leveling off for $z \gtrsim 650$ mm [19]. At a given axial position, the steady state temperature decreases with increasing suspended particle concentration—an indication of heat transfer enhancement as will be discussed later in Section 3.2.

Fig. 8 illustrates the effect of Reynolds number on the dimensionless steady state temperature distribution. Given the suspended particle flowrate, an increase in the Reynolds number gives a lower steady state temperature due to shorter residence time for the fluid phase flowing through the column at higher

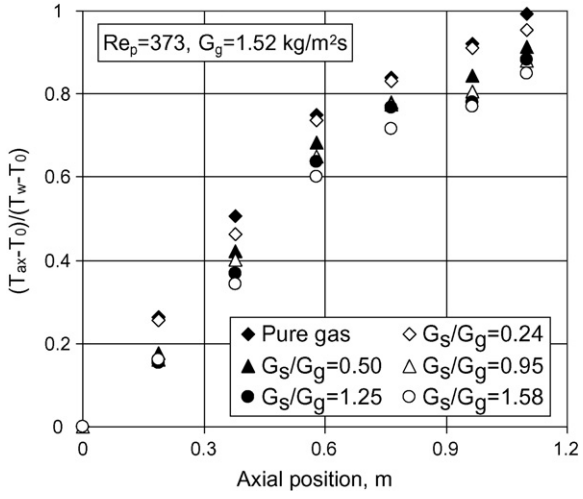

Fig. 7. Axial distribution of the steady state temperature at different solids loadings for $Re_p = 373$, $G_g = 1.52\ \mathrm{kg/(m^2\ s)}$ and 55 μm glass beads.

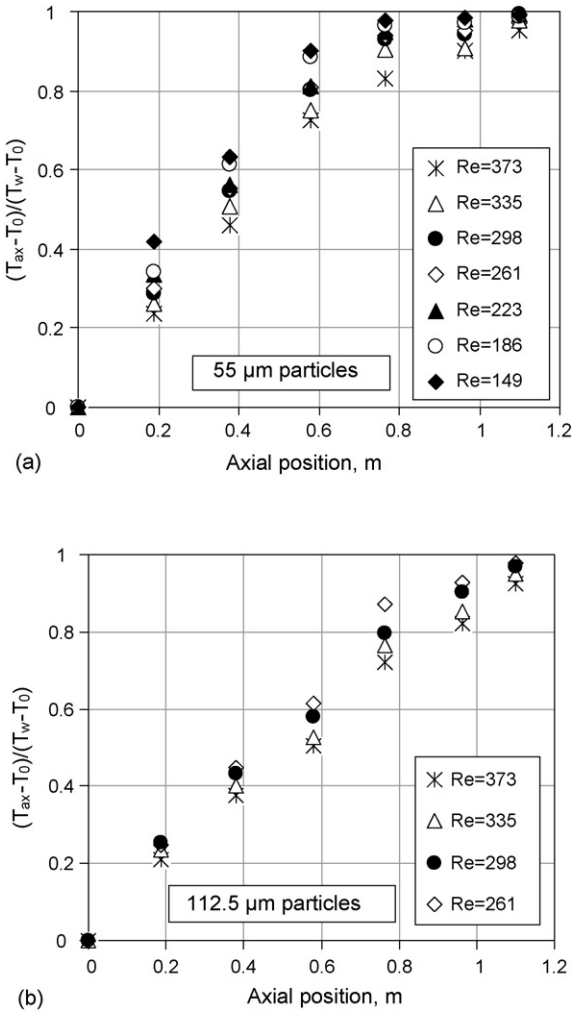

Fig. 8. Effect of Reynolds number on the steady state temperature distribution in the axial direction: (a) 55 μm particles, $G_s = 0.32\,\mathrm{kg/(m^2\,s)}$ and (b) 112.5 μm particles, $G_s = 0.62\,\mathrm{kg/(m^2\,s)}$.

Reynolds numbers; hence, the heat is transported out the column more quickly. A comparison between the data shown in Figs. 7 and 8 show a contradiction—given a particle flowrate, a higher Reynolds number would mean a lower solid-to-gas mass flow ratio, which, according to Fig. 7, would lead to a higher temperature, but Fig. 8 clearly shows a lower temperature. Reasons for such 'contradiction' include: (a) relative importance of the contributions of the gas flow and the suspended particle flow to be discussed later in Section 3.2.2 (Eq. (13)) and (b) different residence times involved in the two cases hence the comparison mentioned above is not entirely adequate.

3.2. Heat transfer coefficient between the packed bed and gas–solid two-phase mixtures

3.2.1. Methodology for the data processing

When a gas–solid two-phase mixture flowing through a packed bed, various heat transfer processes occur. Under the conditions of this work, these processes can be in series or parallel and include convective heat transfer between the column wall and gas phase, column wall and suspended particles, gas phase and the suspended particles, gas phase and packed bed, and suspended particles and packed bed, heat conduction between the column wall and the packed bed, as well as heat conduction within gas, suspended particles and packed particles. Most of these heat transfer processes are also affected strongly by the hydrodynamics of the gas–solid two-phase flow, which is still not currently fully understood [1,21]. It is therefore difficult, if not impossible, to obtain the heat transfer coefficients for each of these processes. This is also the case even for single phase gases flowing through packed beds for which various models based on the effective parameters such as the effective radial thermal conductivity and wall-fluid heat transfer coefficient have to be used; see for example, Ferreira et al. [7], Collier et al. [8] and Wen and Ding [9].

In this work, we will adopt the method used by Royston [15] and Balakrishnan and Pei [16–18] who quantified the convective heat transfer between the packed bed and the flowing gas–solid two-phase mixtures using the concept of the logarithmic mean temperature difference and the heat balance. A brief description of the method and the underlying assumptions are given in the following paragraphs.

Let Q denotes the heat gained by the gas–solid mixture flowing through the packed bed, then

$$Q = m_g c_g[(T_g)_{out} - (T_g)_{in}] + m_s c_s[(T_s)_{out} - (T_s)_{in}] \tag{6}$$

where m_g and m_s are, respectively, the average mass flow rates of gas and suspended particle phases, T_g and T_s the average gas phase and suspended particle phase temperatures, and the subscripts 'out' and 'in' represent the column outlet and column inlet, respectively. Assuming that the gas and the suspended particle phases have the same temperature both at the column inlet and the outlet, then $(T_g)_{in} = (T_s)_{in}$ and $(T_s)_{out} = (T_g)_{out}$, Eq. (6) reduces to:

$$Q = [m_g c_g + m_s c_s][(T_g)_{out} - (T_g)_{in}] \tag{7}$$

At the steady state, the heat gained by the flowing gas–solid two-phase mixture is from the packed bed and the column wall, which can be expressed as:

$$Q = h_m A_{ht} (\Delta T)_{lm} \tag{8}$$

where h_m is the overall heat transfer coefficient between the gas–solid two-phase mixture and the packed bed, A_{ht} the total heat transfer area including both the packed particle and column wall surfaces and $(\Delta T)_{lm}$ is the logarithmic mean temperature difference defined as:

$$(\Delta T)_{lm} = \frac{[(T_{ap})_{in} - (T_g)_{in}] - [(T_{ap})_{out} - (T_g)_{out}]}{\ln[((T_{ap})_{in} - (T_{ap})_{out})/((T_{ap})_{out} - (T_g)_{in})]} \tag{9}$$

where T_{ap} is the average temperature of the packed bed and the column wall. Combination of Eqs. (7)–(9) gives the overall heat transfer coefficient:

$$h_m = \frac{[m_g c_g + m_s c_s][(T_g)_{out} - (T_g)_{in}]}{A_{ht}\{[(T_{ap})_{in} - (T_g)_{in}] - [(T_{ap})_{out} - (T_g)_{out}]\}} \times \ln \frac{(T_{ap})_{in} - (T_g)_{in}}{(T_{ap})_{out} - (T_g)_{out}} \tag{10}$$

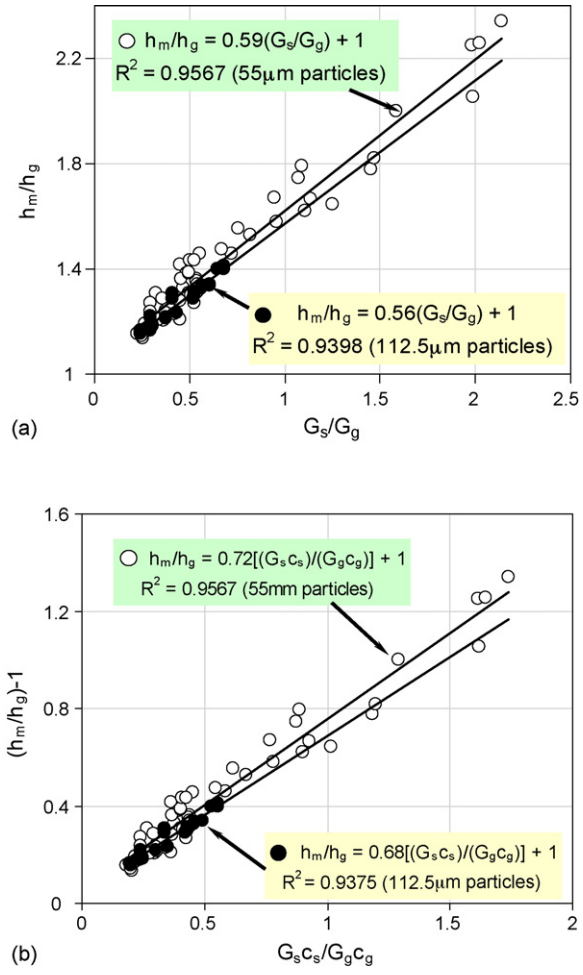

Fig. 9. Dependence of overall heat transfer coefficient enhancement on suspended particle loading and heat capacity ratio: (a) h_m/h_g vs. G_s/G_g and (b) h_m/h_g vs. G_sc_s/G_gc_g.

Insertion of the experimental data into Eq. (10) gives the overall heat transfer coefficient.

The use of LMTD method assumes that the flow and heat transfer are fully developed and that there is no axial dispersion and conduction. These require further validation through careful experiments, which is planned for our future work.

3.2.2. Heat transfer coefficient

Inserting the experimental data into Eq. (10) gives the heat transfer coefficient. Fig. 9 shows the results in the form of h_m/h_g as a function of G_s/G_g (Fig. 9(a)) and in the form of $(h_m/h_g - 1)$ as a function of $(G_sc_s)/(G_gc_g)$ (Fig. 9(b)) for the two sized particles. One can see approximately linear relationships between h_m/h_g and G_s/G_g and between $(h_m/h_g - 1)$ and $(G_sc_s)/(G_gc_g)$, similar to the observation of Royston [15] and Balakrishnan and Pei [18] for constant wall temperature operations. Regression of the data sets gives:

$$\frac{h_m}{h_g} = 0.59\frac{G_s}{G_g} + 1 \tag{11a}$$

$$\frac{h_m}{h_g} = 0.72\frac{G_sc_s}{G_gc_g} + 1 \tag{11b}$$

for the 55 μm suspended particles (regression coefficient, $R^2 = 0.9567$) and

$$\frac{h_m}{h_g} = 0.56\frac{G_s}{G_g} + 1 \tag{12a}$$

$$\frac{h_m}{h_g} = 0.68\frac{G_sc_s}{G_gc_g} + 1 \tag{12b}$$

for 112.5 μm suspended particles (regression coefficient, $R^2 = 0.9398$). A comparison between Eqs. (11a) and (12a) with Eq. (4a), and between Eqs. (11b) and (12b) with Eqs. (1) and (4b) indicates very different pre-factors, which can be reasonably attributed to different operating conditions—constant wall heat flux conditions used in this work while constant wall temperature conditions used by Royston [15] and Wen et al. [19]. The pre-factors of Eqs. (11a) and (12a) are also different from that of Eq. (2) obtained by Balakrishnan and Pei [18] though to a much lesser extent, which will be discussed later.

Eqs. (11a)–(12b) also indicate the heat transfer coefficient ratio decreases with increasing particle size, however, the particle size effect is weak under the conditions of this work, which is consistent with the observations of Royston [15] and Balakrishnan and Pei [18]. It should also be noted that although regression of the data shows the weak effect of particle size, the difference over the same range as the error bar. More work is needed on this, particularly over a much wide size range.

Due to the weak effect of particle size as discussed above, efforts have only been made to relate the Nusselt number (Nu_m) to the Reynolds and Archimedes numbers and particle loading, which is obtained from dimensional analysis [22]. It is found that the following relationship agrees, respectively, within 7 and 11% with the experiments for 112.5 and 55 μm particles (Fig. 10):

$$Nu_m = 0.014Ar_m^{0.25}\ Re_p^{0.5}\left(1 + \frac{G_s}{G_g}\right)^{0.68},$$

$$Re_p = 149\text{–}373 \text{ and } \frac{G_s}{G_g} = 0.2\text{–}2.1 \tag{13}$$

Fig. 11 summaries the measured Nusselt number as a function of Reynolds number at various solid-to-gas mass flux ratios (data points in the upper left part of the figure). Also included are the data obtained by Balakrishnan and Pei [16–18] for $Ar_m = 5.4 \times 10^5$ to 4.3×10^6 and $\Phi_s = 0.85$–1.0 in the upper right part of the figure, as well as the data for the constant wall temperature experiments obtained by Royston [15] and Wen et al. [19] for $Ar_m = 3.4 \times 10^6$ to 3.7×10^6 and $\Phi_s = 1.0$ in the lower part of the figure. It can be clearly seen that the data obtained in this work for the constant wall heat flux conditions are consistent with the results of Balakrishnan and Pei [16–18]. Fig. 11 seems to indicate that the Reynolds number and particle loading have a greater influence on the Nusselt number under the constant heat flux conditions than that under the constant wall temperature conditions. However, a comparison of Eqs. (5) and (13) reveals that the powers of Re and $(1 + (G_s/G_g))$ are the same under the two heating conditions, indicating that the difference is mainly due to the difference in the values of the pre-factors.

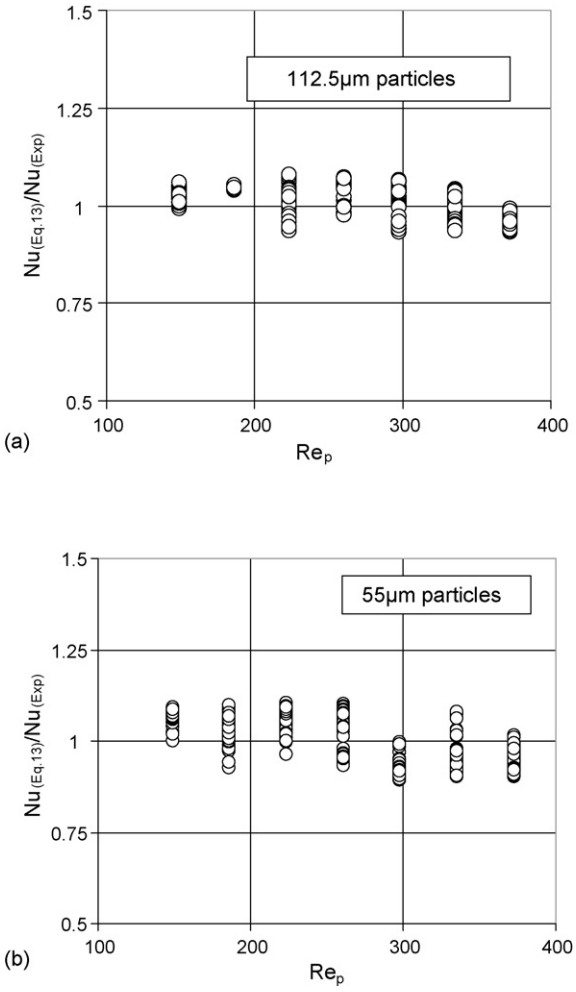

Fig. 10. Comparison of Eq. (13) and experimental results: (a) 112.5 μm particles and (b) 55 μm particles.

The data shown in Fig. 11 suggest that the experimental conditions used by Balakrishnan and Pei [16–18] be most likely under the constant heat flux conditions rather than under the constant wall temperature conditions. This seems to be more logical as the microwave heating device was used by them, which did not seem to have temperature control. Given a power rating, the microwave heating device should provide constant heat to the bed.

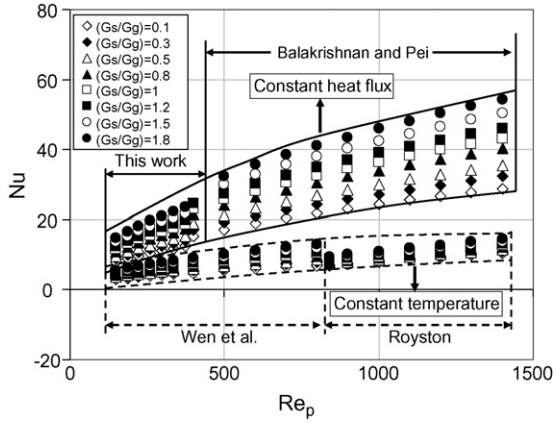

Fig. 11. Nusselt number as a function of Reynolds number and comparison with the literature data for both constant wall temperature and constant wall heat flux conditions.

Fig. 11 shows that the Nusselt number, under the constant wall heat flux conditions, is ~3 times of that under constant wall temperature conditions. This is similar to the well-known results for the fully developed laminar flow through empty tubes, where the Nusselt number for the constant wall temperature conditions is 3.66, whereas that for the constant wall heat flux conditions is 4.36.

Note that although the data obtained in this work fit (Eq. (13)), it is recognized that the equation may not be generic as the data are obtained with fixed column geometry. The changes in other parameters, such as densities and heat capacities of the gas and particle phases, as well as the viscosity of the gas phase are small due to relatively small range of temperature tested in this work. More work is needed to test the generality of the equation.

3.2.3. *Mechanisms of the heat transfer enhancement*

Figs. 9 and 11 clearly show the heat transfer enhancement due to addition of suspended particles. There are a number of mechanisms that could have contributed to the enhancement. First, let us consider a gas–solid two-phase mixture entering a packed bed; the mixture will undergo tortuous routes due to the confinement of the packing. This leads to the suspended particles to interact with each other, with the packed particles and with the column wall. The total length a suspended particle travels through the bed will be significantly longer than the height of the packed bed. These interactions will also modify the paths of the suspended particles frequently hence more turbulence expected in the gas phase. Qualitatively, these factors are known to enhance heat transfer. On the other hand, the suspended particles themselves are actually heat carriers—another mechanism for the convective heat transfer enhancement. Suspended particles may be trapped in the interstices of the packed particles particularly at relatively low superficial gas velocity. However, under the condition of this study, the percentage of the trapped particles is very small [1]. This part of particles increases the packing fraction of the packed bed hence local disturbance of the gas flow which could also enhance the heat transfer. It is well known that packed beds have a non-uniform voidage distribution and the highest voidage occurs at the wall region where more suspended particles are expected to go through [21,23]. Such non-uniformity also creates radial direction flow, which could also be a mechanism for the heat transfer enhancement. Analyses on the temperature profiles at different radial positions in Section 3.1.2 partly support this mechanism. In addition, the presence of suspended particles may disturb the thermal boundary layer surrounding the packed particles and column wall, which can enhance the convective heat transfer.

4. Concluding remarks

Heat transfer of gas–solid two-phase mixtures flowing through a packed bed has been studied under the constant wall heat flux conditions. The following conclusions have been obtained:

- When suspended particles are introduced into a steady state packed bed, a transient process occurs and the length of the transient period depends on the solids loading and the Reynolds number. After the transient period, another steady state is established but it is different from that before the suspended particles are introduced.
- Compared with a pure gas flowing through the packed bed, the introduction of suspended particles greatly enhances the heat transfer process and the enhancement ratio increases approximately linearly with particle loading and the effect of particle size is relatively weak under the conditions of this work.
- The Nusselt number can be well correlated to the Reynolds number, Archimedes number and the suspended particle loading ratio although the range of Archimedes number is very narrow.
- The Reynolds number and particle loading have a greater influence on the Nusselt number under the constant heat flux conditions than that under the constant wall temperature conditions.
- A comparison of the data obtained in this work and those reported in the literature indicates that the results obtained by Balakrishnan and Pei [16–18] were more likely to be under the constant wall heat flux conditions, which explains the discrepancies as stated in Section 1.

Qualitative discussion on the mechanisms of the heat transfer enhancement is also made. However, more detailed experimental, theoretical and modelling studies are needed to clarify the dominant mechanisms. In particular, simultaneous study of both the flow hydrodynamics and heat transfer is needed as the two processes are coupled. This will be investigated in our future work.

Acknowledgements

The authors would like to extend their thanks to EPSRC for financial support under Grants GR/S524985. TNC would like to acknowledge the Vietnamese government for providing a Ph.D. studentship.

References

[1] Y.L. Ding, Z.L. Wang, D.S. Wen, M. Ghadiri, Hydrodynamics of gas–solid two-phase mixtures flowing upward through packed beds, Powder Technol. 153 (2005) 13–22.
[2] D. Kunii, M. Suzuki, Particle-to-fluid heat and mass transfer in packed beds of fine particles, Int. J. Heat Mass Transfer 10 (1967) 845–852.
[3] D.J. Gunn, J.F.C. De Souza, Heat transfer and axial dispersion in packed beds, Chem. Eng. Sci. 29 (1974) 1363–1371.
[4] N. Wakao, S. Kaguei, T. Funazkri, Effect of fluid dispersion coefficients on particle-to-fluid heat transfer coefficients in packed beds: correlation of Nusselt numbers, Chem. Eng. Sci. 34 (1979) 325–336.
[5] J. Shent, S. Kaguei, N. Wakao, Measurements of particle-to-gas heat transfer coefficients from one-shot thermal responses in packed beds, Chem. Eng. Sci. 36 (1981) 1283–1286.
[6] D.E. Beasley, J.A. Clark, Transient response of a packed bed for thermal energy storage, Int. J. Heat Mass Transfer 27 (1984) 1659–1669.
[7] L.M. Ferreira, J.A.M. Castro, A.E. Rodrigues, An analytical and experimental study of heat transfer in fixed bed, Int. J. Heat Mass Transfer 45 (2002) 951–961.
[8] A.P. Collier, A.N. Hayhurst, J.L. Richardson, S.A. Scott, The heat transfer coefficient between a particle and a bed (packed or fluidised) of much larger particles, Chem. Eng. Sci. 59 (2004) 4613–4620.
[9] D.S. Wen, Y.L. Ding, Heat transfer of gas flow through a packed bed, Chem. Eng. Sci. 61 (2006) 3532–3542.
[10] C.A. Depew, T.J. Kramer, Heat transfer to flowing gas–solid mixtures, Adv. Heat Transfer 9 (1973) 113–180.
[11] J. Sun, M.M. Chen, A theoretical analysis of heat transfer due to particle impact, Int. J. Heat Mass Transfer 31 (1988) 969–975.
[12] J.D. Lu, G. Flamant, B. Variot, Theoretical study of combined conductive, convective and radiative heat transfer between plates and packed beds, Int. J. Heat Mass Transfer 37 (1994) 727–736.
[13] Y.L. Shi, A.S. Mujumdar, M.B. Ray, Parametric study of heat transfer in turbulent gas–solid flow in multiple impinging jets, Ind. Eng. Chem. Res. 42 (2003) 6223–6231.
[14] Z. Mansoori, M. Saffar-Avval, H. Basirat Tabrizi, G. Ahmadi, Experimental study of turbulent gas–solid heat transfer at different particles temperature, Exp. Therm. Fluid Sci. 28 (2004) 655–665.
[15] D. Royston, Heat transfer in the flow of solids in gas suspensions through a packed bed, in: Industrial Engineering and Chemistry Proceedings of Design and Development, vol. 10, 1971, pp. 145–150.
[16] A.R. Balakrishnan, D.C.T. Pei, Convective heat transfer in gas–solid suspension flow through packed beds, J. Am. Inst. Chem. Eng. 24 (1978) 613–619.
[17] A.R. Balakrishnan, D.C.T. Pei, Heat transfer in gas–solid packed bed systems, in: Industrial Engineering and Chemistry Proceedings of Design and Development, vol. 18, 1979, pp. 30–51.
[18] A.R. Balakrishnan, D.C.T. Pei, Thermal transport in two-phase gas–solid suspension flow through packed beds, Powder Technol. 62 (1990) 51–57.
[19] D.S. Wen, T.N. Cong, Y.L. Ding, Heat transfer of gas–solid two-phase mixtures flowing through a packed bed, in: Proceedings of the 13th International Heat Transfer Conference and Exposition, Sydney, Australia, 2006.
[20] Z.L. Wang, Y.L. Ding, M. Ghadiri, Flow of a gas–solid two-phase mixture through a packed bed, Chem. Eng. Sci. 59 (2004) 3071–3079.
[21] Y.L. Ding, Z.L. Wang, D.S. Wen, M. Ghadiri, X.F. Fan, D.J. Parker, Solids behaviour in a gas–solid two-phase mixture flowing through a packed particle bed, Chem. Eng. Sci. 60 (2005) 5231–5239.
[22] N.T. Cong, Flow and heat transfer behaviour of gas–solid two-phase mixtures flowing through a packed bed reactor, Ph.D. Transfer Report, University of Leeds, 2006.
[23] S. Li, Y.L. Ding, D.S. Wen, Y.R. He, Modelling of the behaviour of gas–solid two-phase mixtures flowing through packed beds, Chem. Eng. Sci. 61 (2006) 1922–1931.